Unsteady laminar flows of a Carbopol® gel in the presence of wall slip

Antoine Poumaere, Miguel Moyers-Gonzalez, Cathy Castelain, Teodor Burghelea

Unsteady laminar flows of a Carbopol® gel in the presence of wall slip

Antoine Poumaere

LUNAM Université, Université de Nantes, CNRS, Laboratoire de Thermocinétique, UMR 6607, La Chantrerie, Rue Christian Pauc, B.P. 50609, F-44306 Nantes Cedex 3, France

Miguel Moyers-González

Department of Mathematics and Statistics, University of Canterbury, Private Bag 4800, Christchurch, 8041, NZ

Cathy Castelain

Cathy.Castelain@univ-nantes.fr

Teodor Burghelea

LUNAM Université, Université de Nantes, CNRS, Laboratoire de Thermocinétique, UMR 6607, La Chantrerie, Rue Christian Pauc, B.P. 50609, F-44306 Nantes Cedex 3, France

Abstract

We present a comparative experimental study of unsteady laminar flows of a yield stress shear thinning fluid (Carbopol® - 980) in two distinct configurations: a parallel plate rheometric flow and a pressure driven pipe flow. Consistently with the observations in the case of the rheometric flow, the in-situ characterization of the unsteady pipe flow reveals three distinct flow regimes: *solid (plug-like)*, *solid-fluid* and *fluid*. In both configurations and as the flow forcing is gradually increased, the yielding emerges via an irreversible transition. The irreversibility of the deformation states is coupled to the wall slip phenomenon. Particularly, the presence of wall slip nearly suppresses the scaling of the deformation power deficit associated to the rheological hysteresis with the rate at which the material is forced. An universal scaling of the slip velocity with the wall velocity gradients and a slip length which is independent on the degree of the flow steadiness is observed in the pipe flow.

Keywords: physical gel, Carbopol®, yielding, pipe flow, rheological hysteresis, wall slip

1. Introduction

Yield stress fluids represent a broad class of materials made of high molar mass microscopic constituents which display a solid-like behaviour as long as the stress applied onto them does not exceed a critical value called the yield stress, τ_y, and a fluid behaviour beyond this threshold.

The constantly increasing level of interest of both theoreticians and experimentalists in yield stress fluids has, in our opinion, a two-fold motivation. From a practical perspective, such materials have found an increasing number of practical applications for several major industries (which include foods, cosmetics, oil field, etc.) and they are encountered in the daily life in various forms such as food pastes, hair gels and emulsions, cement, mud, etc..

Understanding the unsteady flows of yield stress fluids is important in practical settings including industrially relevant flows of waxy crude oils [19, 30], transport of ice slurries [35], coating flows employed in food industry and geophysical flows.

Email addresses: Miguel.MoyersGonzalez@canterbury.ac.nz (Miguel Moyers-González), Teodor.Burghelea@univ-nantes.fr (Teodor Burghelea)

From a fundamental perspective and even in the case of minimal thixotropic effects, yield stress materials continue triggering intensive debates and posing difficult challenges to both theoreticians and experimentalists. From a historical perspective, the best known discussion is related to the very existence of the yield stress [1, 2]. It was thus suggested that the yield stress is a *engineering* reality rather than a physical one or, in other words, the apparent yield stress behaviour observed during rheological tests is related to a very large Newtonian viscosity rather than to the onset of flow (yielding).

In context of the recent developments of the rheometric equipment (now able to resolve torques as small as $0.1nNm$ and rates of shear as small as $10^{-7}\ s^{-1}$), this debate seems to have reached an end. Indeed, recent and systematic rheological tests performed on various yield stress materials proved unequivocally the existence of a true yielding behaviour, [21, 6, 12].

Whereas there exist numerous compelling investigations of the existence of yield stress, much less work has been done on the dynamics of the yielding transition. Thus, this topic interesting for both theoreticians and experimentalists, particularly in the case of realistic flows which are often unsteady and take place in the presence of wall slip. In practical flow situations involving pasty materials the yielding transition is often associated with the wall slip phenomenon which complicates even further the theoretical description. As in the case of pasty materials the wall slip manifests in a range of small shearing forces one can note that, for such materials, the wall slip and the yielding transition are coupled. This fact brings an additional experimental and theoretical difficulty in exploring the solid-fluid transition and modelling realistic flows of such materials in industrially relevant settings.

Carbopol® gels have been frequently used in many rheological and hydrodynamic experimental studies of the yielding behaviour of viscoplastic fluids. They are synthetic polymers of acrylic acid initially introduced over six decades ago (B.F. Goodrich Co.). They are cross-linked with various chemical compounds such as divinyl -glycol, allyl-sucrose, polyalkenyl polyether etc.. Addition of a neutralising agent (e.g. sodium hydroxide, $NaOH$) leads to a decrease in the number of the positive hydrogen ions H^+ resulted from the dissociation of the polyacrylic acid in a polar solvent such as the water. The un-compensated sodium ions Na^+ lead to an increase of the osmotic pressure and the individual polymer particles swell dramatically. Consequently, for polymer concentrations exceeding a threshold value c^* (overlap concentration), the swollen polymer particles jam forming a micro-gel system which can locally sustain finite deformations (behaving like an elastic solid) prior to damage. When the locally applied stresses exceed a threshold value the micro gel system breaks apart and the material starts to flow. This is the commonly accepted microscopic scale origin of the macroscopic yielding of a Carbopol® gel.

Due to their low thixotropy, excellent micro-structural stability, optical transparency and highly reproducible and stable rheological properties, the Carbopol® gels been considered for over a decade a *model yield stress fluids*, [10, 27].

It has only recently been shown that in a range of low applied stresses and depending on the manner they are force these materials may actually depart from an ideal viscoplastic picture and that around the yield point thixotropic effects and irreversible deformation states may be observed, [15, 14, 32].

In contrast to the large number of studies of the yielding of Carbopol® gels in rheometric flows, the body of literature concerning experimental studies of the solid-fluid transition of Carbopol® gels in industrially relevant flows is, to our best knowledge, more limited. An experimental study of the yielding and flow properties of a 0.2% Carbopol® in a capillary tube has been performed by González and his coworkers, [29]. By combining classical rotational rheometry techniques with Digital Particle Image Velocimetry (**DPIV**) measurements of steady flows driven at various pressure drops the authors present a detailed experimental characterisation of the yielding process and the flow patterns. As the driving pressure drop is gradually increased, they observe a smooth solid-fluid transition rather than a sharp one and correctly identify this as one of the factors that lead to uncertainties in the determination of the yield stress. To overcome the difficulty of accurately measuring the yield stress triggered by the smoothness of the solid-fluid transition, the authors of the study propose an alternative method of measuring this parameter based on the analysis of the measured velocity profiles, [29]. As the flows studied in Ref. [29] were stationary, this work did not capture the dynamic coupling (in unsteady flow conditions) between yielding and wall slip which, in part, motivates the present study.

Ma and his coworkers reported an experimental investigation of pipe flows of a petroleum-coke sludge slurry in the presence of wall slip, [19]. They assess the wall slip behaviour using the Mooney method and correlate the slip behaviour with both the rheological properties of the slurries and the driving pressures.

The body of existing literature on unsteady pipe flows of Carbopol® gels is, to our best knowledge, quite limited

which inherently limits the extent of this bibliography review.

A theoretical study of the dispersion of a solute in the pulsatile pipe flow of a yield stress fluid was recently presented by Nagarani and Sebastian, [23]. Using the Casson model, they demonstrate that the periodic flow of the fluid contributes significantly to the total dispersion process compensating for the effect of the yield stress.

The development of the laminar unsteady pipe flow of a thixotropic fluid was studied by Corvisier and his coworkers, [8]. By measuring the flow fields via the Particle Image Velocimetry technique, they have found a clear coupling between the kinetics of the micro-structural changes and the evolution of the flow.

Park and his coworkers have studied oscillatory flows of a 0.075% Carbopol® solution in a acrylic made U-shaped tube with a circular cross section, [28]. A compelling experimental evidence of the significant role played by the elasticity on the measured unsteady velocity profiles (particularly near the centreline of the flow channel) is provided. Due to the elastic effects associated to the presence of un-yielded bands in the flow, strongly nonlinear time histories of the strain are recorded. To model their experimental findings, Park and his coworkers propose an elasto-viscoplastic model which fits their data better than the regularised Bingham model. Some discrepancies between theory and experiment still exist and may be due to the fact that their model does not account for the velocity slip near the wall.

The aim of the present study is to present a detailed comparative experimental characterisation of laminar unsteady flows of a Carbopol® gel in two distinct flow configurations: a rheometric flow between parallel disks and a pressure driven pipe flow.

The paper is organised as follows. The experimental setup, the measuring technique and the physical and rheological properties of the solutions are detailed in Sec. 2. The experimental results are presented in Sec. 3. A systematic description of the solid-fluid transition observed in a rheometric flow with a particular emphasis on the role of wall slip and its coupling to the irreversibility of the deformation states is presented in Sec. 3.1. A detailed characterization of inertia-free unsteady pipe flows of a Carbopol® solution is presented in Sec. 3.2. The paper closes with a discussion of our main findings, of their impact on the current understanding of flows of yield stress fluids, Sec. 4. Several directions worth being pursued by future studies will also be discussed.

2. Experimental setup and methods

2.1. Preparation and characterisation of the Carbopol® solutions

A 0.08% (by weight) solution of Carbopol® 980 has been used as a working fluid. The procedure for the preparation of the solution is described as follows. First, the right amount of anhydrous Carbopol® 980 has been gently dissolved in water while continuing stirring the mixture with a commercial magnetic stirring device. The stirring process was carried on until the entire amount of polymer was homogeneously dissolved. A particular attention has been paid to the homogeneity of the final mixture, which has been assessed visually by monitoring the refractive index contrast of the mixed solution. Next, the pH of the mixture (initially around 3.2, due to the dissociation of the polyacrylic acid in water) has been brought to a neutral value by addition of about 140 parts per million (ppm) of sodium hydroxide ($NaOH$). The final value of the pH has been carefully monitored using a digital pH- meter (from Grosseron).

2.2. Rheological measurement protocol

The rheological properties of the solutions were investigated using a Mars III (from Thermofischer) rheometer equipped with a Peltier system able to control the temperature with an accuracy better than $0.1^{\circ}C$ and a nano-torque module which allows one to accurately explore very small rates of deformation, $\dot{\gamma} \approx 10^{-5}\ s^{-1}$.

To quantitatively assess the role of the wall slip on the unsteady yielding process, two alternative geometries have been used: a smooth parallel plate system and a serrated one. The radius of each geometry was $R = 35\ mm$ and the gap between the parallel plates was $d = 1\ mm$. Measurements of flow curves performed with the rough parallel plate system for various gaps indicated that the plate's roughness did suffice to prevent the wall slip (data not shown here). A detail description of the method/procedure can be found in Ref. [39].

To prevent the artefacts related to the evaporation of the sample during long runs, a solvent trap has been placed around the free fluid meniscus. The sealing of the solvent trap on the base plate of the rheometer has been insured by a thin layer of vacuum grease. After each experimental run it has been carefully checked (by visual inspection)

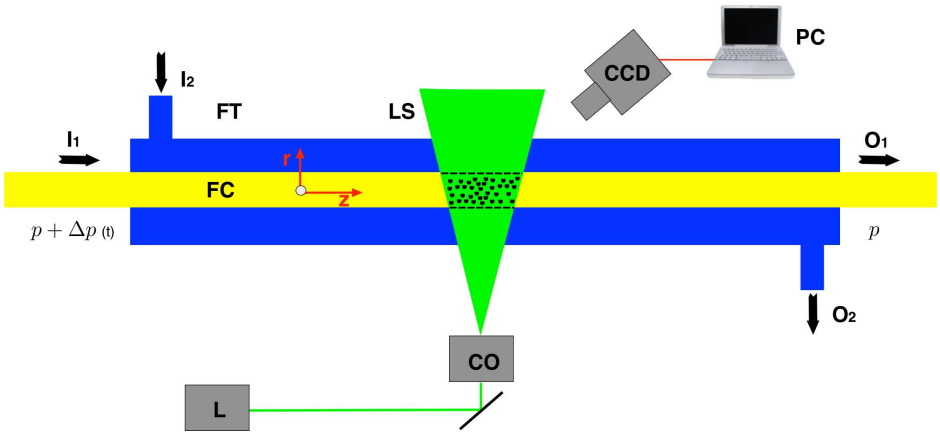

Figure 1: Schematic view of the experimental apparatus: **FT** - fish tank, $\mathbf{I_2}$ - water inlet, $\mathbf{O_2}$ - water outlet, **FC** - flow channel, $\mathbf{I_1}$ - working fluid inlet, $\mathbf{O_1}$ - working fluid outlet, **L** - solid state laser, **CO** - cylindrical optics block, **LS** - laser sheet, **CCD** - digital camera, **PC** - personal computer.

that no significant changes in the shape of the meniscus occurred. Additionally, we have checked at the end of each run that one can reproduce the viscosity measured during the pre-shear step which indicated us that the evaporation effects were either minimal or absent.

2.3. Experimental apparatus and methods

The experimental setup is schematically illustrated in Fig. 1. It consists of a flow channel **FC** of length $L = 115\ cm$ with a circular cross-section of inner radius $R = 1.9\ mm$.

The flow channel is housed by a acrylic made fish tank **FT** filled with water circulating at a constant temperature, $T = 23^oC$. Besides its role in maintaining a constant operating temperature, the water circulation around the flow channel also provides a good matching of the refractive index which minimises the optical distortions induced by the curved surface of the flow channel.

A green laser beam ($\lambda = 514\ nm$) with a power of 500 mW emitted by the solid state laser **L** (from Changchun Industries, Model LD-WL206) is deflected by a mirror through a cylindrical optics block **CO** which reshapes it into a horizontal laser sheet, Fig. 1. The cylindrical optics block is composed of a glass rod with a short focal distance $f_1 \approx 2\ mm$ and a cylindrical lens with a larger focal distance, $f_2 \approx 5\ cm$. The two optical elements are mounted orthogonally to each other and in a telescopic arrangement such that the primary horizontal laser sheet generated by the glass rod in the $(r-z)$ plane (see Fig. 1) is focused in a direction orthogonal to this plane in the middle of the flow channel by the second lens minimising thus its thickness in the measurement region.

The thickness of the generated laser sheet is roughly $80\mu m$ in the beam waist region which was carefully positioned at the centre line of the flow channel. The working fluid was seeded with an amount of 200 parts per million (ppm) of polyamide particles with a diameter of 60 μm (from Dantec Dynamics). A time series of flow images is acquired with a 12 bit quantisation digital camera **CCD** (Thorlabs, model $DCU224C$) through a $12X$ zoom lens (from La Vision). The resolution of the acquired images is $1280X1024$ pixels which insures a spatial resolution of $2.96\mu m$ per pixel.

A slow controlled pressure flow has been generated by controlling the hydrostatic pressure difference between the inlet and the outlet of the flow channel as schematically illustrated in Fig. 2. The working fluid is held in a container **IFC** with a large free surface rigidly mounted on a vertical translational stage **TS**. The translational stage is vertically driven by a step motor **M** via a gear box **GB**.

The position and the speed of the stepping motor are controlled by a micro-step controller (model IT 116 Flash from Isel Gmbh) connected to a personal computer **PC** via a RS 232 serial interface. To control the motion of the stepping motor, a graphical user interface (GUI) has been developed under Matlab®. The vertical position of the inlet fluid container **IFC** is controlled with an accuracy of $\Delta h_0 = 37\ \mu m$. After passing through the flow channel, the fluid is collected in a outlet fluid container **OFC** placed on a digital balance **B**. The balance provides real time readings of the mass of the fluid discharged through the channel and estimate the pressure drop in the connecting tubing. The pressure driving the pipe flow is $p(t) = \rho g h(t) - p_t$ where $\rho = 1050\ kg\ m^{-3}$ is the density of the Carbopol® solution,

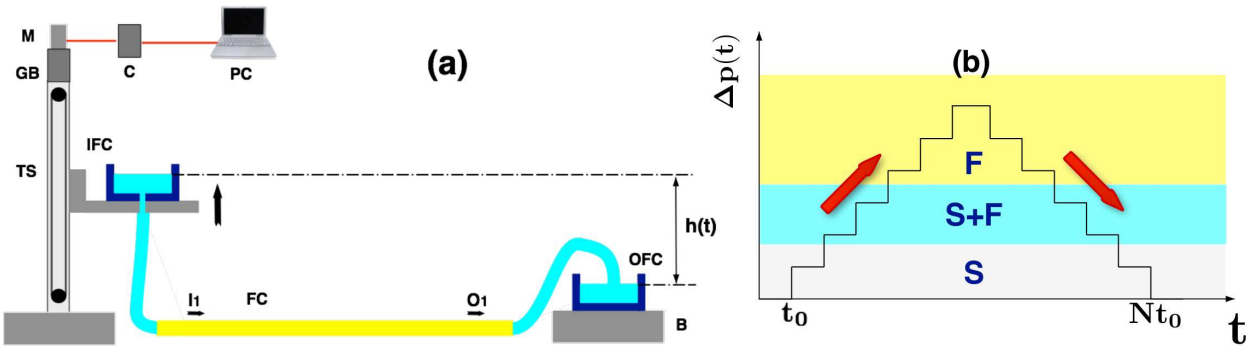

Figure 2: **(a)** Schematic view of the flow control system: **TS** - vertical translational stage, **M** - stepping motor, **GB** - gear box, **GB** - micro step controller, **PC** - personal computer, **IFC** - inlet fluid container, **OFC** - outlet fluid container, **FC** - flow channel, **FC** - flow channel, $\mathbf{I_1}$ - working fluid inlet, $\mathbf{O_1}$ - working fluid outlet, **B** - digital balance. **(b)** Schematical representation of the hydrostatic pressure ramp. t_0 is the characteristic forcing time (the averaging time per stress point) and N is the total number of steps. The symbols marking the highlighted regions denote the deformation regimes and are explained in the text: **(S)** - solid, **(S+F)** - solid- fluid coexistence, **(F)** - fluid.

g the acceleration of gravity and p_t the pressure drop in the connecting tubes. The resolution in the hydrostatic pressure corresponding to the micrometric step of the motor was $\Delta p_0 = \rho g h_0 \approx 0.37 Pa$. The imposed hydrostatic pressure closely mimics the flow ramps employed in Ref. [32] to investigate the yielding phenomenon and consisted of linear hydrostatic pressure ramps for both increasing and decreasing values of the height difference $h(t)$, Fig. 2 (b). As illustrated in Fig. 2 (b), it consists of N individual steps each lasting a time t_0 which will further be referred to as the *characteristic forcing time*. Time series of the velocity fields were obtained by a iterative multi-grid Digital Particle Image Velocimetry (**DPIV**) algorithm implemented in the house under Matlab® [37, 34]. For this purpose, simultaneously with the hydrostatic pressure ramp illustrated in Fig. 2(b) a sequence of flow images has been acquired at a frequency of 10 frames per second (fps). Corresponding to low values of the driving pressure, several flow images have been skipped in order to increase the inter-frame and maintain the average displacement of the tracer particles in the optimal range of 5 to 15 pixels, [34, 37]. Together with this, the smallest interrogation window has been adapted to the mean flow velocity corresponding to each step of the pressure ramp. The spatial resolution of the measured flow fields was 99.5 μm.

3. Experimental results

3.1. Unsteady yielding in a rheometric flow: the role of wall slip

Prior to characterising the unsteady pipe flow of a Carbopol® gel we focus on the solid-fluid transition which observed in an unsteady rheometric flow between parallel plates. It is known that Carbopol® gels exhibit slip while flowing past smooth surfaces, [31]. This motivated us to perform a comparative rheological investigation of a Carbopol® gel in two separate geometries with and without wall slip.

The rheological response of the Carbopol® sample to an externally applied stress is probed by performing an unsteady stepped stress ramp performed at a constant temperature. This stress ramps closely mimics the pressure ramp that drives the channel flow illustrated in Fig. 2(b). The rationale of the choice of this rheological protocol is to be able to correlate the rheological measurements with the flow measurements performed in the channel which follow a similar forcing scheme. The protocol is schematically illustrated in the insert of Fig. 3(a). During each step of the ramp the stress applied onto the sample is maintained constant a finite time t_0. After reaching a maximal value purposely chosen to correspond to a fully yielded deformation regime, the stress is gradually decreased through the same intermediate values in order to probe the reversibility of the deformation states.

The results of the measurements performed with both rough plates and smooth plates are presented in Fig. 3(a).

The choice of representing the rheological data in the coordinates $|\dot{\gamma}| = \dot{\gamma}(\tau)$ is motivated by the fact that this dependence is single valued on both the increasing and the decreasing branch of the stress ramp and therefore allows a more accurate identification of the various deformation regimes.

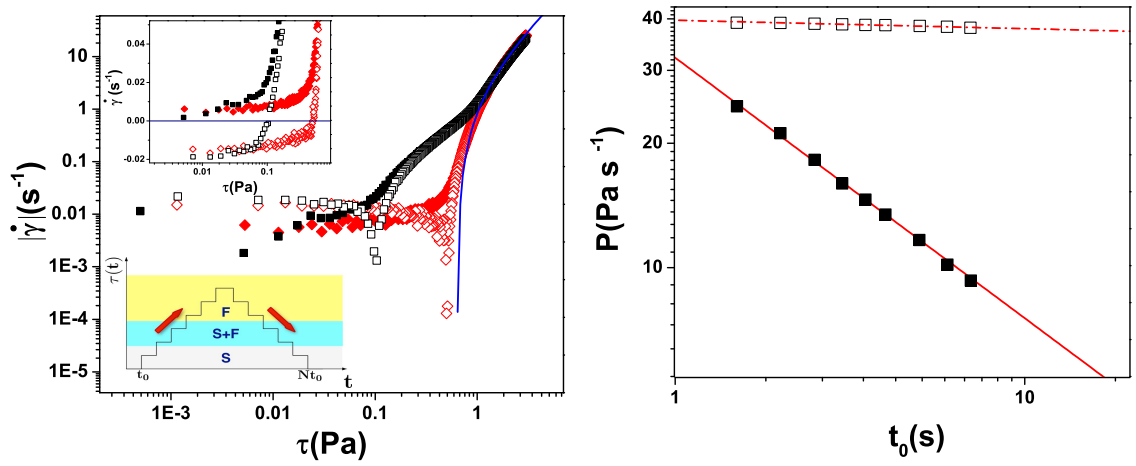

(a) (b)

Figure 3: (a) Flow curves measured with a polished geometry (□, ■) and with a rough geometry (◇, ♦). The full/empty symbols refer to the increasing/decreasing branch of the flow curves. The full line is a Herschel-Bulkley fit that gives $\tau_y = 0.64 \pm 0.003(Pa)$, $K = 0.4 \pm 0.002(Pas^n)$, $n = 0.54 \pm 0.001$. A magnified view of the solid-fluid transition is presented in the upper insert. The controlled stress unsteady stress ramp is schematically illustrated in the lower insert. The symbols marking the highlighted regions denote the deformation regimes and are explained in the text: **(S)** - solid, **(S+F)** - solid- fluid coexistence, **(F)** - fluid. (b) Dependence of the hysteresis area on the characteristic forcing time t_0 measured with a smooth geometry (□) and a rough one (■). The full line (−) is a guide for the eye, $P \propto t_0^{-0.63}$ and the dash dotted line (−.−) is a guide for the eye, $P \propto t_0^{-0.03}$.

In the absence of wall slip (the rhombs in Fig. 3(a)) and for low values of the applied stress ($\tau \leq 0.64Pa$) the absolute value of measured rate of deformation $|\dot{\gamma}|$ is constant on both branches (increasing/decreasing) of the stress ramp and, consequently, the strain γ is a linear function of the applied stresses which is the signature of a elastic solid deformation regime. Note that the stress ramp is linear in time as illustrated in Fig. 2 and, therefore, one can conclude that the material deforms as an elastic solid within this regime, $G = \tau/\gamma = ct$.

Within this regime the deformation states are not reversible upon increasing/decreasing applied stresses which translates into different elastic moduli: $G_u > G_d$. Here the indices denote the increasing/decreasing stress ramps, respectively.

For large values of the applied stresses ($\tau \geq 0.64Pa$) a reversible fluid regime is observed. One has to emphasise that the transition from a irreversible solid like deformation regime to a reversible fluid one is not direct, but mediated by an intermediate deformation regime which can not be associated with neither a solid like behaviour nor a fluid one but with a coexistence of the two phases. A similar smooth solid-fluid transition has been recently observed in a low Reynolds number steady pipe flow, [29].

An interesting flow feature can be observed on the decreasing branch of the pressure ramp in the form of a cusp of the dependence of $|\dot{\gamma}|$ on the applied stress (the empty rhombs in Fig. 3(a)). Corresponding to this point, the shear rate changes its sign. To better see this effect, we re-plot a magnified view of the cusp region in a linear scale in the upper insert. This effect may be understood in terms of an elastic recoil manifested through a change in the direction of rotation of the top disk.

The irreversibility of the deformation states observed within the solid and the intermediate deformation regimes and initially reported by Putz et al in [32] has been recently confirmed by others, [15, 13, 14]. A similar irreversible rheological behaviour has been found in rheological studies performed on various grades of Carbopol® gels using various rheometers (and various geometries) at various temperatures, [22, 38].

We note that, during each of the rheological measurements reported in this manuscript and in our previous studies [32, 22, 38], the Reynolds number was smaller than unity, therefore the experimentally observed irreversibility of the deformation states illustrated in Fig. 3(a) should not be associated with inertial effects.

To gain further insights into the role of wall slip in the unsteady yielding of the Carbopol® gel, we have performed the same type of rheological measurements with smooth parallel plates (the squares in Fig. 3(a)). The main effect of

the wall slip is to shift the solid-fluid coexistence regime to lower values of the applied stresses in Fig. 3(a)). The apparent yield stress measured in the presence of wall slip τ_y^a is nearly an order of magnitude smaller than the yield stress measured in the absence of slip, τ_y. The data acquired with and without wall slip overlap only within the fluid regime, corresponding to shear rates $\dot{\gamma} > \dot{\gamma}_c$ (with $\dot{\gamma}_c \approx 0.8s^{-1}$ see Fig. 3(a)). This critical value of the shear rate above which the slip and no slip data overlap is comparable to the critical shear rate found by Bertola and his coworkers below which no steady state flow could be observed by MRI, [3]. The existence of the critical shear rate $\dot{\gamma}_c$ is also consistent with the measurements of the velocity profiles performed by Salmon and his coworkers with a concentrated emulsion sheared in a small gap Couette geometry, [36].

Additionally, we note that it is solely within the viscous deformation regime that all the data sets can be reliably fitted by the Herschel-Bulkley model (the full line in Fig. 3(a)) which reinforces the idea that only within this deformation range the Carbopol® gel behaves like a simple or "model" yield stress fluid.

A next fundamental question that deserves being addressed is how the irreversible character of the rheological flow curves observed within the solid-fluid coexistence regime in the form of a hysteresis loop is related to the rate at which the deformation energy is transferred to the material or, in other words, to the characteristic forcing time t_0. It is equally important to understand if (and how) the presence of wall slip influences this dependence. To address this points we compare measurements of the area of the hysteresis of the dependence $|\dot{\gamma}| = |\dot{\gamma}(\tau)|$ observed in the flow curves presented in Fig. 3(a) $P = \int_{\tau_i}^{\tau_{\max}} \left(\dot{\gamma}^u - |\dot{\gamma}^d|\right) d\Delta\tau$ performed for various values of t_0 for both slip and no-slip cases. Here the indices "u,d" refer to the increasing/decreasing stress branches of the flow ramp, τ_i is the stress corresponding to the intersection of the two branches and τ_{max} the maximal applied stress. As already discussed in Ref. [32] the area P has the dimensions of a deformation power deficit per unit volume of sheared material. The results of these comparative measurements are presented in Fig. 3(b). In the absence of wall slip, the deformation power deficit scales with the characteristic forcing time as $P \propto t_0^{-0.63}$.

The existence of a rheological hysteresis for Carbopol® gels characterised by a decrease of the power deficit with the characteristic forcing time consistent with [14, 32].

In the absence of slip and in the limit of very slow forcing ($t_0 \to \infty$) the hysteresis vanishes and the deformation states are fully recoverable upon increasing/decreasing forcing. This scaling indicates that, within the solid deformation regimes, steady states of deformation can be reached only after significant times which is consistent with the results by Moller and his coworkers, [21].

Whereas the emergence of the hysteresis behaviour observed in the absence of the wall slip is certainly related to and depends upon the unsteadiness of the forcing (the value of t_0), the scaling behaviour of the power deficit, $P \propto t_0^{\alpha}$, is related to the molecular structure of the material. Thus, for various materials (various grades of Carbopol® gels, bentonite gels at various concentrations, carbon black suspensions, mayonnaise) different scaling exponents α have been measured, [32, 14].

Together with the obvious remark that the hysteresis behaviour is observed in the same range of the driving stresses as the solid-fluid transition, one can conclude that this behaviour emerges from the coupling of the unsteady flow forcing and the local dynamics of the solid and fluid material elements (bands) in the transitional region which is directly related to the structural properties of the material.

To probe the coupling between the hysteresis behaviour and the wall slip, similar measurements of the hysteresis area P for various values of t_0 have been performed in the presence of wall slip (the empty symbols in Fig. 3(b)). It is found that the wall slip affects both the magnitude of the deformation power deficit and its scaling with the characteristic forcing time by nearly suppressing it: $P \propto t_0^{-0.03}$ (the dash-dotted line Fig. 3(b)).

This new scaling of the rheological hysteresis loses with the degree of flow steadiness provides the first quantitative evidence that a true steady state of deformation is practically impossible to achieve in the presence of wall slip. Indeed, the low values of the scaling exponent indicates that reaching a steady state of the flow in the presence of wall slip (the hysteresis vanishes) practically requires huge waiting times t_0 which are significantly larger than any time scale associated to a rheological test.

3.2. Unsteady yielding in a laminar unsteady pipe flow in the presence of wall

Following the comparative investigation of the yielding of a Carbopol® gel in a rheometric flow in the presence and in the absence of wall slip presented in Sec. 3.1, the main question that arises is to what extent the findings on the solid-fluid transition investigated in a classical rheometric flow could be transferred to flows that are more relevant from a practical perspective, such as a laminar unsteady pipe flow in the presence of wall slip.

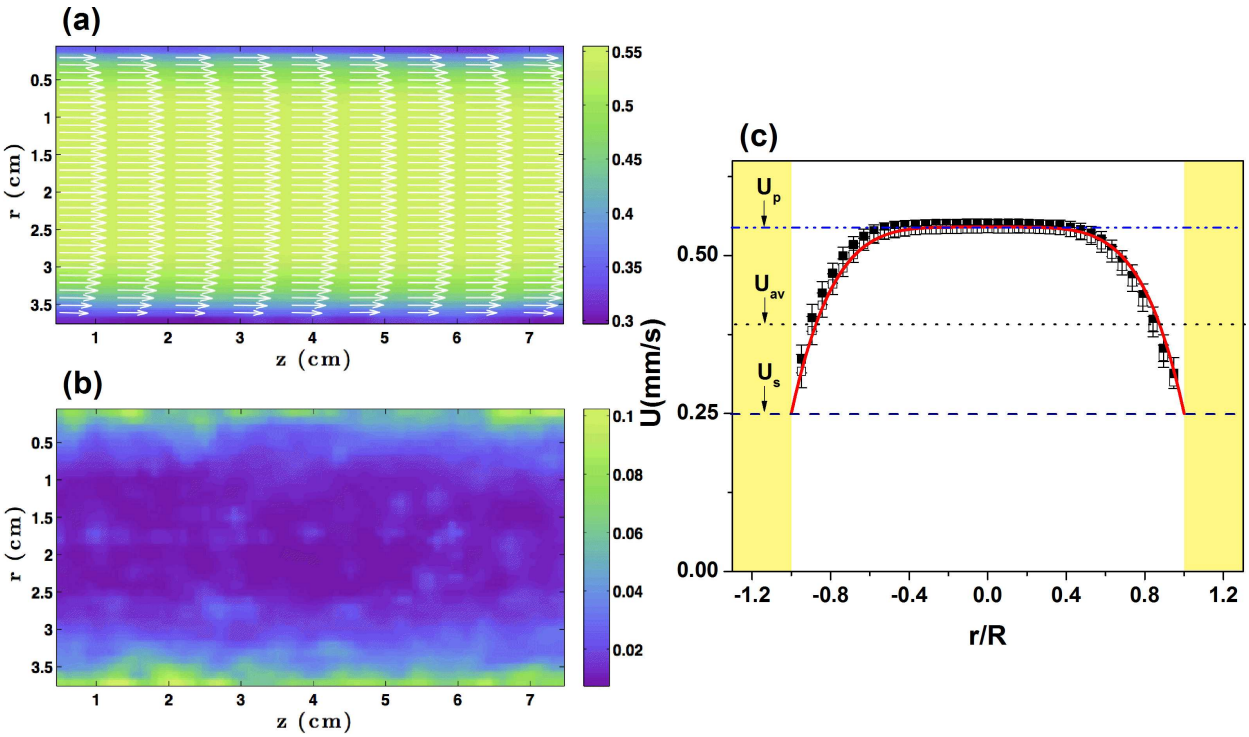

Figure 4: **(a)** Time averaged (over 100 instantaneous fields) velocity field. The false colour map refers to the modulus of the velocity. **(b)** Reduced velocity fluctuations, U^{rms}/U. **(c)** Time averaged velocity profiles measured for $\Delta p = 1300\ Pa$ on the increasing (full symbols) and decreasing (empty symbols) branch of the pressure ramp. The error bars are defined by the root mean square deviation (rms) of the velocity. The full line is a fit by the analytical solution defined by Eq. 1. The velocity data were acquired after a steady state was achieved, $t_0 = 300\ s$. The lateral highlighted regions in panel (c) refer to the walls of the flow channel.

To characterise the solid-fluid transition in the unsteady channel flow in the presence of the wall slip, a time series of flow fields has been acquired during a controlled increasing/decreasing pressure ramp (see Fig. 2(b)). This controlled pressure ramp closely mimics the controlled stress ramps used to characterise the solid-fluid transition in a rheometric flow.

Choosing a large value of the characteristic forcing time t_0 allows one to study the limiting steady state case. For $t_0 = 300\ s$ a typical laminar viscoplastic plug-like flow is observed, Fig. 4(a).

The velocity fluctuations observed in the steady case are solely of an instrumental nature and do not exceed several percents of the time averaged velocity in the bulk but approach 10% in the boundary, Fig. 4(b). The transverse profile of the time averaged velocity displayed in Fig. 4(c) also reproduces well the laminar and steady flow behaviour of a viscoplastic fluid in a tube. Following [11] and in the framework of the Herschel-Bulkley model the profile can be fitted by:

$$U(r) = U_s + \begin{cases} \left(\frac{n}{n+1}\right)\left(\frac{1}{2K}\cdot\frac{\Delta p}{L}\right)^{\frac{1}{n}}(R-R_p)^{\frac{1}{n}+1}, |r| < R_p \\ \left(\frac{n}{n+1}\right)\left(\frac{1}{2K}\cdot\frac{\Delta p}{L}\right)^{\frac{1}{n}}(R-R_p)^{\frac{1}{n}+1}\left[1-\left(\frac{r-R_p}{R-R_p}\right)^{\frac{1}{n}+1}\right], \textit{otherwise} \end{cases} \tag{1}$$

Here U_s is the slip velocity and R_p is the radius of the un-yielded plug. The slip velocity was measured by extrapolating the nonlinear fit given by Eq. 1. We have used a classical Levenberg-Marquardt nonlinear fitting procedure implemented under Matlab and the reliability of the fitting results has been checked by comparing the values obtained for the power law index and the consistency with those obtained from the rheological measurements.

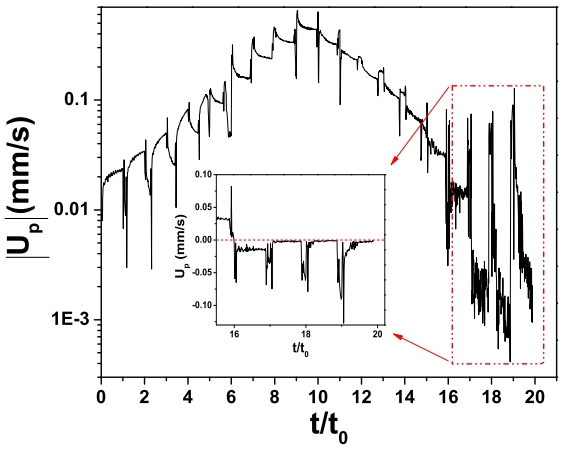

Figure 5: Time series of the absolute value of the plug velocity $|U_p| = |U|\Big|_{r=0}$. The insert presents a magnified view of the time series plotted in a linear scale after the elastic recoil effect is observed (see the text for the explanation). The characteristic forcing time was $t_0 = 7.5s$.

The transverse profiles of the time averaged velocity are reproducible upon increasing/decreasing the pressure drop consistently with a reversible flow regime, Fig. 4(c). These measurements confirm that in the limit of very slow forcing (large t_0) the flow can be correctly described by a Herschel-Bulkley model with wall slip and thus the well known steady state result is recovered.

We now turn our attention to the case when the forcing is unsteady. To characterise the flow response to a unsteady forcing (finite values of t_0) we first monitor the time series of the absolute value of the plug velocity $|U_p|$, Fig. 5 measured during a controlled pressure ramp for a finite value of the characteristic forcing time, $t_0 = 7.5\ s$.

The spikes visible in the velocity time series presented in Fig. 5 are related to the switch of the driving pressure realised by the displacement of the vertical translational stage (**TS** in Fig. 2(a)) which carries the inlet fluid container **IFC**. Their magnitude depends on the inertia of the mechanical system and the acceleration of the stepping motor **M**. To avoid accounting for this response of the mechanical system which controls the pressure drop along the flow channel, the flow data acquired during these transients (extended over roughly $0.5s$ in each of the experiments reported here) has been always discarded and no conclusions were drawn based on it.

For low values of the driving pressure on the increasing branch of the ramp the time (in the range $t/t_0 < 3$) dependence of the centreline velocity does not reach a steady state during the characteristic forcing time $t_0 = 7.5s$.

A further increase of the driving pressure (corresponding to $t/t_0 \in [3,6]$ in Fig. 5) reveals an interesting feature of the velocity time series in the form of a non-monotonic time dependence: upon the change of the pressure drop, the centreline velocity first decreases and then increases. A phenomenological explanation of this observation may be given in terms of a strong heterogeneity of the flow, i.e. a dynamic coexistence and competition between yielding of solid material elements (or bands) and their re-combination which, as illustrated by the rheometric data presented in Fig. 3(a), occurs within an intermediate range of the applied stresses (pressure drops). Indeed, as the driving pressure drop Δp is further increased, this non-monotonic behaviour is no longer observed and the plug velocity reaches a steady state during a characteristic time smaller than t_0. This indicates that, within this range of driving pressure, a steady yielded state is achieved, Fig. 5.

The time series presented in Fig. 5 may also provide a first indication on the reversibility of the flow states upon increasing/decreasing the driving pressure drops. Thus, one can note that the data is not symmetric with respect to the vertical line $t/t_0 = 10$. This observation is consistent with the irreversibility of the deformation states observed for the rheological data acquired at low and intermediate values of the applied stresses, Fig.3(a). An even clearer signature of the irreversibility of the deformation states can be noted if one monitors the time series data acquired during the last four steps of the decreasing branch of the pressure ramp and highlighted in the insert of Fig. 5. During these steps of the pressure ramp the velocity fluctuates strongly and, corresponding to the the last steps, a flow reversal is apparent: the plug velocity velocity changes sign as the pressure drop is decreased to its smallest value. This rather

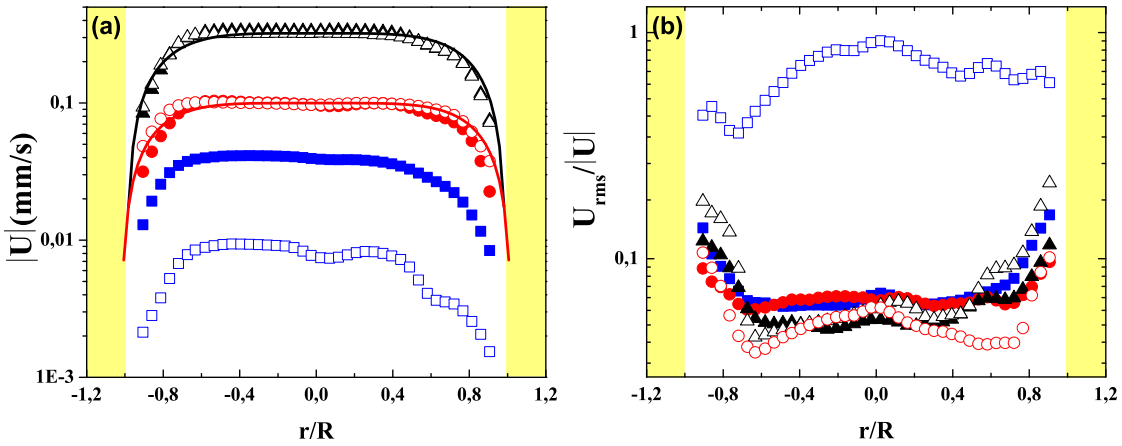

Figure 6: (a) Profiles of the absolute value of the time averaged flow velocity $|U|$. The full lines are the fit functions by the analytical solution defined by Eq. 1. (b) Profiles of the reduced root mean square variation of the velocity, $\frac{U_{rms}}{|U|}$. The symbols refer to different values of the pressure drop: (□,■) - $\Delta p = 310.8Pa$, (○,●) - $\Delta p = 621.6Pa$, (△,▲) - $\Delta p = 932.3Pa$. The full/empty symbols refer to the data acquired on the increasing/decreasing branch of the pressure ramp, respectively. The lateral highlighted regions in both panels refer to the walls of the flow channel. The characteristic forcing time is $t_0 = 10s$.

unexpected effect can be associated to a elastic recoil effect similar to the elastic recoil observed during the rheological measurements on the decreasing stress branch and manifested by the cusp visible in Fig. 3(a).

Profiles of the absolute value of the time averaged flow velocity U and the reduced velocity fluctuation U_{rms}/U measured for several values of the driving pressure Δp on both the increasing and the decreasing branch of the flow ramp are presented in Fig. 6.

For each value of the driving pressure, a central unyielded plug of the time averaged profile of the axial velocity can be observed on the increasing branch of the flow ramp, Fig. 6. In this regards, the velocity profiles are similar to the steady state ones illustrated in Fig. 4(c) and can be formally fitted as well by Eq. 1. For each value of the pressure drop, a slip behaviour can be clearly observed near the channel walls, $r/R = \pm 1$. For the largest values of the driving pressure ($\Delta p = 932.3Pa$ and $\Delta p = 621.6Pa$, in Fig. 6 (a))) the velocity profiles measured on the increasing/decreasing branches of the ramp are consistent with a reversible and flow behaviour. Within this flow regime the velocity fluctuations quantified by U_{rms}/U_{av} are the smallest and they are mainly localised near the channel wall which is another indicator for the steadiness of the flow (see Fig. 6 (b)).

At low driving pressures the flow reversibility is broken: the profile measured on the decreasing branch in Fig. 6 (a) falls clearly below the profile measured on the increasing pressure branch.

It is equally worth noting that, corresponding to this driving pressure, the mean flow profile is less smooth around the centreline of the channel which indicates a rather large level of velocity fluctuations. It also indicates that smaller the driving pressure is further the flow is from a steady state.

To probe this hypothesis we turn our attention to the transverse profiles of the reduced velocity fluctuations U_{rms}/U_{av}, Fig. 6 (b)). For large driving pressure, the reduced velocity variations account for roughly 6% of the mean flow velocity in the bulk region of the flow (around the unyielded plug) and they may reach up to 20% of the mean flow velocity in the wall region (due to the smallness of the measured velocity). The rather large values of the fluctuations observed near the channel walls are instrumental and they are due to the smallness of the measured velocity within this regions (here, the **DPIV** heavily relies on the sub-pixel interpolation because of the very small displacements of the flow tracers).

On the decreasing branch of the controlled pressure ramp and for low driving pressures a localisation of the velocity fluctuations can be observed in the form of a local maximum centred around the middle of the channel

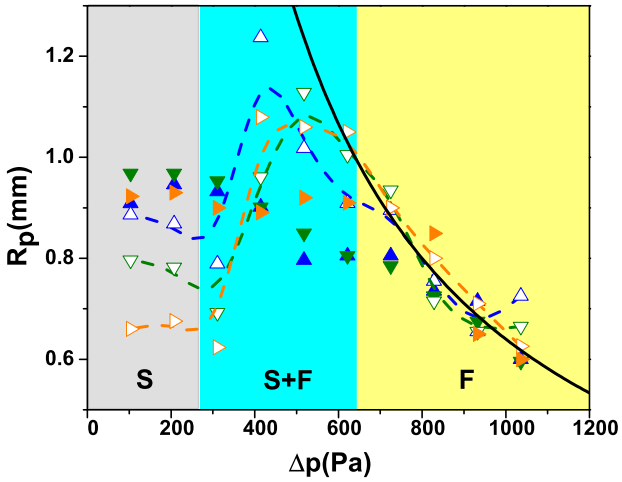

Figure 7: Dependence of the plug radius R_p on the driving pressure drop Δp for various values of the characteristic forcing time t_0 : ($\triangle, \blacktriangle$) - $t_0 = 4s$, ($\triangledown, \blacktriangledown$) - $t_0 = 7.5s$, ($\triangleright, \blacktriangleright$) - $t_0 = 15s$. The full/empty symbols refer to the data acquired on the increasing/decreasing branch of the pressure ramp, respectively. The full line is the Herschel - Bulkley prediction, $R_p = \frac{0.64}{\Delta p}$. The symbols marking the highlighted regions denote the deformation regimes and are explained in the text: **(S)** - solid, **(S+F)** - solid- fluid coexistence, **(F)** - fluid.

$(r/R = 0)$ can be observed. The localisation of the velocity fluctuations near the centre line of the flow channel may be interpreted in terms of large fluctuations of an elastic (unyielded) plug which is consistent with the experimental findings for the case of a oscillatory pipe flow, [28].

The measurements of the time averaged transverse profiles of the axial velocity allow one to quantify the extend of the elastic solid plug. To do this within the solid (**S**) and solid-fluid (**S-F**) flow regimes, the transverse velocity profiles have been formally interpolated by spline functions which permit the calculation of their derivatives. The extrapolation of the spline functions at the walls of the channel allows one to estimate the magnitude of the slip velocity. The plug regions have been defined in relation to the instrumental error of the **DPIV** measurements by the loci of the points for which the absolute value of the numerical derivative does not exceed 5% of its maximal value (typically measured near the solid wall of the flow channel). For large driving pressure drops (within the fluid deformation regime (**F**)), the flow profiles can be fitted by Eq. 1 and the same procedure of determining the slip velocity and plug size used for the steady state case can be applied. The dependence of the plug radius R_p on the driving pressure drop Δp measured for various values of the characteristic forcing time t_0 on both the increasing and the decreasing branch of the controlled pressure ramp is presented in Fig. 7. At low values of the pressure drops on the increasing branch or the flow ramp the plug radius is practically independent on the driving pressure. This is consistent with a rigid body downstream motion of the core un-yielded fluid: the shear stresses associated with the yielded wall layers can not overcome the bulk yield stress of the fluid and the size of the plug is insensitive to the changes in the driving pressure. Beyond a critical value of the pressure drop Δp_y a monotone decrease of the plug radius is observed and, according to [9], this dependence can be fitted by $R_p = 2L\tau_y^a/\Delta p$ which leads to $\tau_y^a \approx 0.27Pa$. This value of the apparent yield stress is close to the apparent yield stress measured in a rheometric flow in the presence of wall slip, Fig. 3. The plug radius data acquired on the decreasing branch of the pressure ramp reproduces the data acquired on the increasing branch only within the yielded regime, $\Delta p > \Delta p_y$. This once again indicates that the flow states are irreversible around the yield point, in agreement with the rheological measurements presented in Fig. 3. On the decreasing branch of the flow ramp (the empty symbols in Fig. 7), the values of the plug radius pass through a local maximum before reaching an elastic solid plateau. This effect may be related to the elastic recoil effect primarily observed on the decreasing stress branch of the rheological flow ramp (the cusp in Fig. 3) and thereon highlighted in the insert of Fig. 5.

Within the framework of the Herschel-Bulkley model and in the absence of the wall slip, the mean flow velocity U_{av} is related to the driving pressure drop via:

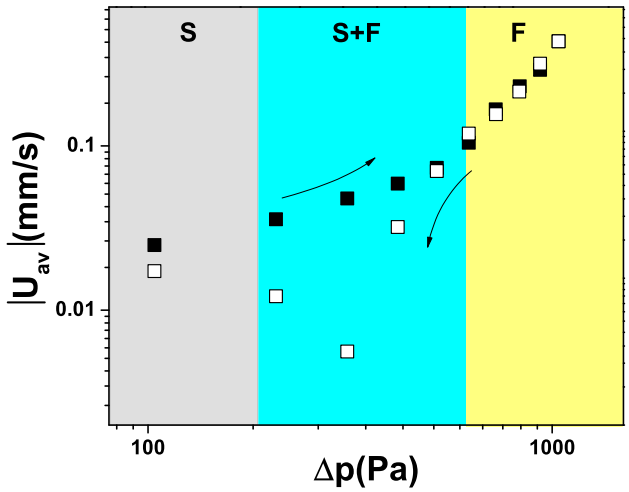

Figure 8: Dependence of the absolute value of the mean flow velocity U_{av} on the applied pressure drop Δp. The characteristic forcing time was $t_0 = 4s$. The full/empty symbols refer to the increasing/decreasing branch of the linear controlled stress ramp. The symbols marking the highlighted regions denote the deformation regimes and are explained in the text: **(S)** - solid, **(S+F)** - solid- fluid coexistence, **(F)** - fluid.

$$U_{av} = \begin{cases} 0, & \xi \leq 1. \\ \left[\frac{R\Delta p}{LK}\right]^{1/n} \frac{R}{2+1/n}\left[1-\frac{1}{\xi}\right]^{1+1/n}\left[1+\frac{1}{\xi(1+1/n)}\right], & \xi > 1. \end{cases} \tag{2}$$

see e.g. [5]. The dimensionless parameter ξ is defined:

$$\xi = \frac{R\Delta p}{2L\tau_y} \tag{3}$$

The Eq. 2 relies heavily on the Herschel-Bulkley yielding picture, the flow steadiness and the absence of velocity slip at the channel's wall. Although we expect that none of these assumptions is fully fulfilled by the flow we investigate, we still believe it is reasonable to use it in order to get just an indicator for order of magnitude for the applied pressure drop that corresponds to yielded states, Δp_y, which would ultimately indicate us a suitable range of the driving pressure drops Δp that needs to be explored during our experiments in order to systematically characterise the solid-fluid transition for this type of unsteady pipe flow.

Using the yielding criterion $\xi \approx 1$ the pressure drop corresponding to the yielded (flowing) states can be estimated as $\Delta p_y \approx 774Pa$.

Measurements of the absolute value of the mean flow velocity U_{av} performed for increasing/decreasing values of the driving pressure Δp and several values of the characteristic forcing time are presented in Fig. 8. The mean flow velocity U_{av} has been calculated by numerical integration of the **DPIV** measured velocity profiles, $U_{av} = 2\pi \int_0^R rU(r)dr$ [1].

The mean velocity data acquired for increasing/decreasing driving pressures overlap only within the fluid regime $\Delta p > \Delta p_y$. This indicates that only corresponding to this range the Carbopol® gel is fully yielded. Below this critical value of the driving pressure a hysteresis of the flow states is observed. These observations are fully consistent with the rheological hysteresis observed in the presence of wall slip (the squares in Fig. 3(a)). As previously mentioned through our paper, the cusp visible on the decreasing pressure branch corresponds to a elastic recoil effect manifested by a reversal of the flow direction. This indicates that, as in the case of the solid-fluid transition observed in a rheometric flow [32], the elasticity cannot be ignored while studying the unsteady yielding in a slow pipe flow of a Carbopol® gel.

[1] The axial symmetry of the flow has been assumed.

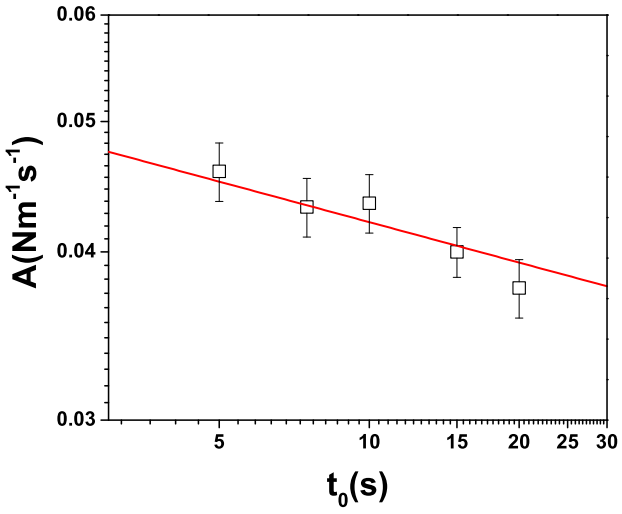

Figure 9: Dependence of the area of the hysteresis of the dependencies of the mean flow velocity on the driving pressure drop presented in Fig. 8 on the characteristic forcing time t_0. The full line is a guide for the eye, $A \propto t_0^{-0.1}$.

The dependence of the area of the hysteresis observed in the dependence of the mean flow velocity U_{av} on the driving pressure Δp illustrated in Fig. 8 defined by $A = \int U_{av}^{u} d\Delta p^{u} - \int |U_{av}|^{d} d\Delta p^{d}$ is presented in Fig. 9. The absolute value appearing in the second term of the expression above is explained by the fact that, on the decreasing branch of the ramp, the velocity may become negative due to an elastic recoil effect manifested within the solid-fluid coexistence regime.

As in the case of the rheological hysteresis in the presence of slip illustrated in Fig. 3(b) a weak dependence of the hysteresis area on the characteristic forcing time is observed, $A \propto t_0^{-0.1}$.

This fact indicates that the presence of wall slip modifies the irreversibility of the flow curves within the solid-fluid coexistence regime and prompts us to focus closer on the slip behaviour observed during the stepped pressure ramp and its relation to the rheological behaviour illustrated in Fig. 3.

The dependence of the slip velocity U_s obtained by extrapolation of either the fit of the velocity profile or its interpolant on the driving pressure drop Δp measured for several values of the characteristic forcing time t_0 is presented in Fig. 10.

As in the case of the pressure dependence of the mean flow velocity U_{av} illustrated in Fig. 8 and discussed above, one can clearly see in Fig. 10 that the dependence of the slip velocity on the applied pressure drop Δp is not reversible upon increasing/decreasing pressure over the entire range of pressures. The results holds for all the values of the characteristic forcing time t_0 (data not show here) and represents another indicator that the slip behaviour can not be entirely decoupled from the irreversible solid-fluid transition observed during the rheological measurements presented in Fig. 3(a).

Regardless the value of the characteristic forcing time t_0, within the fluid flow regime ($\Delta p > 500Pa$) the slip velocity scales with the applied pressure drop as $U_s \propto \Delta p^2$ (see the full lines in Fig. 10). This scaling law differs from the one found by González and his coworkers in [29], $U_s \propto \Delta p^{0.876}$ (see Fig. 6 in Ref. [29] in connection to their Eq. (3)). As the scaling law we found is practically insensitive to the characteristic forcing time, we believe that this discrepancy is not related to the degree of steadiness of the pipe flow investigated in [29] but to the different rheological properties of the Carbopol® solutions they have used (nearly an order of magnitude difference in both the yield stress and the consistency). Based on this comparison, it is apparent that even within the reversible fluid regime ($\tau > \tau_y$) the wall slip behaviour remains correlated to the rheological properties of the solution.

To get a deeper insight into this correlation, we focus on the dependence of the slip velocity U_s on the wall velocity gradients $\left.\frac{\partial U}{\partial r}\right|_{r=\pm R}$, Fig. 11. The measurements presented in Fig. 11 are performed for various values of the

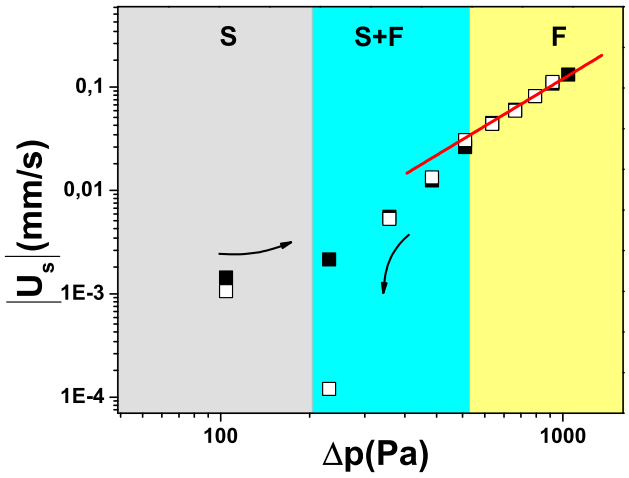

Figure 10: Dependence of the slip velocity U_s on the applied pressure drop Δp . The characteristic forcing time was $t_0 = 20s$. The full/empty symbols refer to the increasing/decreasing branches of the stress ramp, respectively. The full line is guides for the eye, $U_s \propto \Delta p^2$. The symbols marking the highlighted regions denote the deformation regimes and are explained in the text: **(S)** - solid, **(S+F)** - solid- fluid coexistence, **(F)** - fluid.

characteristic forcing time t_0 on both the increasing and the decreasing branch of the pressure ramp (see Fig. 2 (b)).

For each of the data sets presented, the wall velocity gradients have been obtained by numerical differentiation of either the fit defined by Eq. 1 or the interpolation of the time averaged velocity profiles near the wall and the slip velocity has been obtained by extrapolating the same fitted profile or its interpolation (see Fig. 6 (a)) at the wall, $r/R = \pm 1$. To increase the accuracy of the numerical differentiation, a central difference differentiation scheme has been used.

Previous studies have reported a decrease of the slip velocity with the applied stresses (velocity gradients) beyond the yield-point, [24]. Contrarily to this, our experimental findings indicate a monotone increase of the slip velocity with the wall velocity gradients, regardless the deformation regime (solid, fluid or solid-fluid) and the degree of flow steadiness (the value of t_0). This conclusion is consistent, however, with the experimental findings for the case of a steady pipe flow, [29].

Regardless the deformation regime, the value of the characteristic forcing time t_0 and the type of the pressure ramp (increasing or decreasing pressures) a universal dependence of the slip velocity U_s on the wall velocity gradients $\left.\frac{\partial U}{\partial r}\right|_{r=\pm R}$ is observed, Fig. 11, and all the data follow a line who's slope indicates a slip length of roughly $300\mu m$ (the full line in Fig. 11) [2].

Thus, one can conclude from theses measurements that the dependence of the slip velocity on the wall velocity gradients has an universal character and uniquely defines a slip length which is independent on the deformation regime but may depend on the roughness of the channel wall and on the physicochemical properties of the Carbopol® solution. Two natural but fundamental questions arise at this point:

1. *What is the extent of this universal behaviour?*
2. *Is there a simple phenomenological picture underlying the wall slip behaviour observed for a Carbopol® gel?*

A first phenomenological picture for the wall slip phenomenon (observed in suspensions) has been suggested in early $20's$ by Bingham by the following quote: *"Slip comes from a lack of adhesion between the material and the shearing surface. The result is that there is a layer of liquid between the shearing surface and the main body of the suspension"*, see page 231 in Ref. [4].

[2] Due to level of scatter related to the errors introduced by the numerical differentiation of the velocity profiles near the channel wall, the data presented in Fig. 11 was not fitted by a power law and the full line should be solely regarded as a guide for the eye.

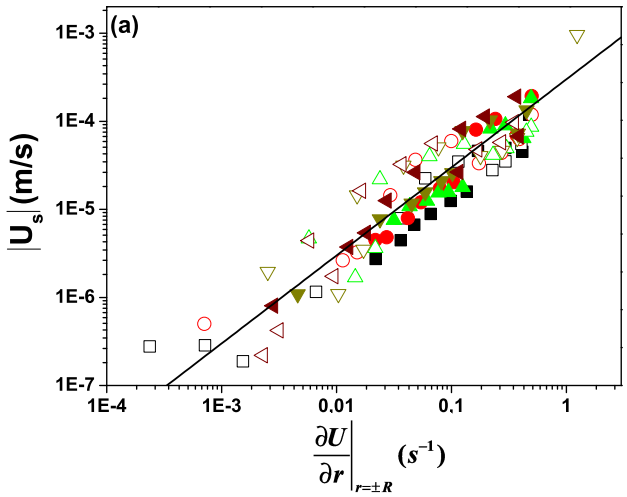

Figure 11: Dependence of the absolute value of the slip velocity $|U_s|$ on the wall velocity gradients. The full line is a guide for the eye, $U_s \approx 3 \cdot 10^{-4} \left.\frac{\partial U}{\partial r}\right|_{r=\pm R}$. The symbols are: (△, ▲) - $t_0 = 4\ (s)$, (○, ●) - $t_0 = 7.5\ (s)$, (□, ■) - $t_0 = 10\ (s)$, (▽, ▲) - $t_0 = 15\ (s)$, (◁, ◀) - $t_0 = 20\ (s)$.

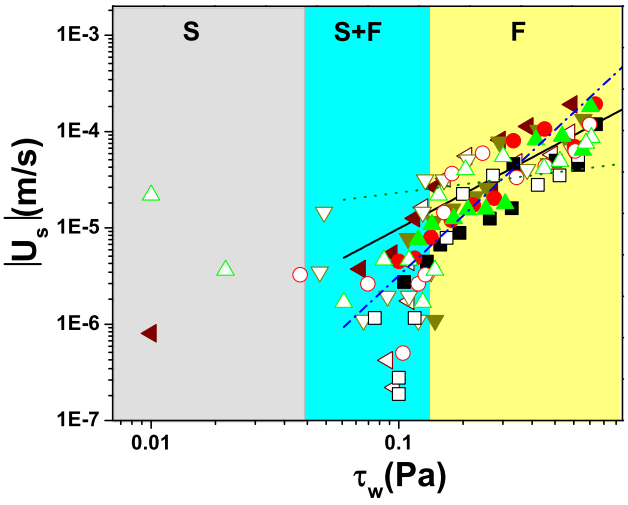

Figure 12: Dependence of the absolute value of the slip velocity $|U_s|$ on the wall shear stresses τ_w. The full line is a power law fit, $U_s = 2.3 \cdot 10^{-4} (\pm 5.4 \cdot 10^{-5}) \cdot \tau_w^{1.32 \pm 0.26}$. The dotted and the dash-dotted lines are the theoretical predictions by Piau (see Ref. [31]): $U_s \propto \tau_w^{1/3}$, $U_s \propto \tau_w^2$. The symbols are: (△, ▲) - $t_0 = 4\ (s)$, (○, ●) - $t_0 = 7.5\ (s)$, (□, ■) - $t_0 = 10\ (s)$, (▽, ▲) - $t_0 = 15\ (s)$, (◁, ◀) - $t_0 = 20\ (s)$. The symbols marking the highlighted regions denote the deformation regimes and are explained in the text: **(S)** - solid, **(S+F)** - solid- fluid coexistence, **(F)** - fluid.

Kaylon developed further on the slip picture suggested by Bingham and proposed the following relationship between the slip velocity and the wall shear stress, [18]:

$$U_s = \beta \left(\tau_w\right)^{1/n_s} \tag{4}$$

The slip coefficient β is related to the width δ of the slip layer, the consistency K_s and power law index n_s of the interstitial fluid arrested within the slip layer (referred to in Ref. [18] as the *"binder fluid"*) via $\beta = \frac{\delta}{K_s^{n_s}}$.

Carbopol® micro gels are not suspensions in the strict sense of the term but they can still be viewed as a jammed system of swollen gel micro-particles, [31]. Thus, bearing in mind that the gel was prepared in an aqueous solvent, it looks reasonable to us to consider the *"binder fluid"* as Newtonian, $K_s = 1\ mPas, n_s = 1$.

To test the applicability of Eq. 4 with the assumptions above for our data, we re-plot the slip velocity data presented in Fig. 11 versus the wall shear stress defined by $\tau_w = \frac{\partial U}{\partial r}\Big|_{r=\pm R} \cdot \eta \left(\frac{\partial U}{\partial r}\Big|_{r=\pm R}\right)$. For this purpose we have related the wall velocity gradients measured by numerical differentiation of the **DPIV** measured velocity profiles to the wall shear stresses via the rheological flow curve measured in the presence of wall slip and presented in Fig. 3(a) (the squares) with the wall velocity gradient playing the role of the rate of shear $\dot{\gamma}$. The result of this evaluation is presented in Fig. 12. Within this representation the universality observed in Fig. 11 is broken and three different slip regimes can now be clearly observed. Corresponding to values of the wall shear stress significantly smaller then the apparent yield stress measured in the presence of wall slip ($\tau_w < \tau_y^a \approx 0.1Pa$, see Fig. 3(a)) the measured slip velocity displays a rather large scatter, most probably related to the smallness of both the slip velocity and wall velocity gradients. However, in spite of this data scatter and as wall shear stress approaches the apparent yield stress τ_y^a measured in the presence of wall slip, the observed behaviour is a reminiscent of the cusp observed in the dependence of the rate of shear on the applied stress presented in Fig. 3(a). This behaviour clearly departs from a Navier-like slip behaviour and it is related to the non-trivial yielding process illustrated in Fig. 3(a) which occurs via an intermediate range of stresses where the solid and fluid phases coexist, [32]. Above the apparent yield stress and corresponding to the fluid deformation regime a nearly linear scaling of the slip velocity with the wall shear stress is observed, $U_s \propto \tau_w^{1.32\pm0.26}$ (the full line in Fig. 12). This indicates a Navier-like slip behaviour which can be described by Eq. 4. This nearly linear scaling reinforces the assumption above that the *"binder fluid"* is Netwonian, i.e. $n_s \approx 1$. We note that a similar scaling law has been found in the recent micro-flow experiments by Gonzalez and his coworkers, [29] (see Fig. 6 in their paper): $U_s \propto \tau_w^{0.876}$. The pre-factor of this linear dependence is $\beta \approx 0.00023\ mPa^{-1}s^{-1}$ which leads to an estimate for the thickness of the Newtonian shear layer $\delta \approx 0.23\mu m$. This estimate is fairly close to the value measured by Jiang and his coworkers for the case of hydroxypropyl guar (HPG) gel, $\delta \approx 0.1\mu m$.

It is interesting to compare our experimentally found scaling of the slip velocity with the theoretical prediction of Piau for a Carbopol® gel presented in Ref [31]. Using a Hertzian framework to model the contacts between neighbouring micro-gel elastic particles (a detailed description of the theoretical framework can be found in Ref. [17]), Piau predicts two scaling laws of the slip velocity with the wall shear stress depending on the packing of the soft particles: $U_s \propto \tau_w^2$ for a closely packed system and $U_s \propto \tau_w^{1/3}$ in the case of a loosely packed system. The scaling exponent obtained by fitting the data presented in Fig. 12 corresponding to the fully yielded regime differs from these theoretical predictions (see the dotted and the dash-dotted lines in Fig. 12).

A possible reason of this discrepancy might originate in the fact that the interstitial lubricating fluid considered in Ref. [31] was non-Newtonian and, to get a deeper insight into the slip behaviour of Carbopol® gels a additional discussion of this issue is in order. A physical rationale for the choice of a non-Newtonian (shear thinning) interstitial fluid in Ref. [31] might be to decouple at a micro scale the shear thinning behaviour (by attributing it to the interstitial fluid) from the yield stress behaviour by implicitly attributing it to the elastic-solid Carbopol® micro particles.

The disagreement we pointed out above seems to indicate that this decoupling is not as straightforward and should be more cautiously considered in future attempts to theoretically describe the relation between flow properties, wall slip and microstructure. Future theoretical approaches should definitely reconsider this problem.

A more elaborated theory of the slip dynamics observed in a soft gel was presented by Meeker and his coworkers, [20]. Due to the non-negligible level of scatter of the data presented in Fig. 12 induced by the numerical differentiation of the measured velocity profiles, however, a direct comparison of our results with these predictions is not possible.

Currently, there exist no experimental studies of the microscopic scale dynamics of Carbopol® gels under shear in the vicinity of slippery surfaces able to confirm the existence of a shear lubricating layer and provide a quantitative

measure of its thickness. Thus, the estimate of the width δ of the lubrication layer we have obtained indirectly from the analysis slip velocity data should only be regarded as plausible. A direct experimental investigation by fluorescent visualization of the gel network as recently performed by Gutowski et al [16] would be highly needed to test this estimates. We can, however, provide some additional arguments for the meaningfulness of this estimate as follows.

Systematic microfluidic investigations of the diffusion of nano-tracers within a Carbopol® micro-gel indicate that the average characteristic size of gel micro particles is of the order of $R_{av} \approx 1\mu m$, [26, 25]. A width of the shear layer $\delta \approx 0.23R_{av}$ together with the assumption of a random close packing of the micro-gel particles is consistent with a rough standard deviation of the particle size $R_{std}/R_{av} \approx 23\%$. Again, based on the microscopic experimental evidence presented in Refs. [26, 25] such a value can be considered, at least for now, plausible.

To conclude this part, our experimental data seems to confirm that in a fluid state ($\tau > \tau_y^a$) the Bingham inspired phenomenological picture of a slip layer proposed by Kaylon is applicable to the unsteady pipe flow of the Carbopol® gel investigated through our paper.

Another important fact that needs to be pointed out regarding the data presented in Fig. 12 is that, regardless the value of the characteristic forcing time t_0 and for both increasing/decreasing values of the driving pressure Δp (the full/empty symbols in Fig. 12, respectively), the slip velocity data overlap onto a single master curve. This invariance of the slip velocity data with the characteristic forcing time t_0 can be explained by the weak dependence on t_0 of the rheological flow curves measured in the presence of wall slip illustrated in Fig. 3(b) which consequently translates into a weak dependence of the hysteresis of the measured mean flow speed illustrated on t_0 (see Fig.9).

To conclude this part, in the case of a unsteady low Reynolds number flow of a Carbopol® solution, the slip behaviour can not be decoupled from solid-fluid transition. Future theoretical developments should account for this experimental fact.

4. Conclusions, outlook

An experimental investigation of the slow yielding of a Carbopol® gel in both a unsteady rheometric flow between parallel and in an unsteady and inertia-free unsteady pipe flow is presented.

The first part of our study presented in Sec. 3.1 dealt with a detailed experimental investigation of the solid-fluid transition of a Carbopol® gel observed during unsteady flow ramps performed in a parallel plate geometry mounted on the rotational rheometer.

In the presence of wall slip, the solid-fluid transition occurs earlier, i. e. the apparent yield stress measured in the presence of slip τ_y^a is nearly an order of magnitude smaller than the yield stress measured in the absence of wall slip, τ_y (see Fig. 3(a)). This result is invariant with respect to the degree of flow steadiness and agrees with previous measurements of steady-state flow curves.

In both the slip and the no slip case the transition from a solid behaviour to a viscous one (fully yielded) is not direct but mediated by an intermediate solid-fluid coexistence regime. The cusp visible within the solid-fluid coexistence regime on the decreasing branch of the stress ramp is associated to a elastic-recoil effect manifested by a flow reversal. In both the slip and the no slip cases the solid-fluid transition is not reversible upon increasing/decreasing of the applied stresses and a hysteresis is clearly visible (see Fig. 3(a)). The presence of wall slip nearly suppresses the scaling of the deformation power deficit P with the rate at which the material is forced, $1/t_0$. This result is noteworthy as it highlights that in the presence of slip a steady deformation state is practically impossible to achieve during time intervals which are relevant to a rheological experiment.

The irreversible solid-fluid transition and the wall slip are observed within the same range of applied stresses indicating that the two phenomena are coupled.

The second part of our study presented in Sec. 3.2 concerns with a systematic experimental investigation of low Reynolds number unsteady pipe flows of a viscoplastic fluid (Carbopol®-980). By means of the **DPIV** technique a full characterisation of the flow fields during controlled stepped ramps of the driving pressure (Fig. 2 (b)) is made. Depending on the value of the applied pressure several flow regimes are observed.

Corresponding to the lowest values of the driving pressure Δp a solid like flow regime is observed. This regime is characterised by a an elastic solid plug which never reaches a steady flow state. The largest level of fluctuations of the solid plug is observed near the centre line of the flow channel which we interpret as the signature of an unsteady solid (elastic) plug.

For the largest values of the driving pressure Δp a fluid regime is observed. Within this regime the velocity reaches a steady state (see Fig. 5) and the flow is reversible upon increasing/decreasing pressures, Figs. 8, 10. As in the case of the rheometric flow discussed in Sec. 3.1, the transition between the solid-like regime to the fully yielded regime is not direct but mediated by an intermediate solid-fluid coexistence regime. For each value of the characteristic forcing time t_0 we have explored, this intermediate phase coexistence regime manifests itself by a clear hysteresis (observed upon increasing/decreasing the driving pressure drop) which is qualitatively similar to the hysteresis observed in the rheological flow curves. The experimentally observed hysteresis of the flow curves is associated with a deformation power deficit and measurements of this quantity for various values of t_0 reveal no sensitive dependence on the frequency of forcing, $A \propto t_0^{-0.1}$ (see Fig. 9). This fact is fully consistent with the measurements of the deformation power deficit performed in a rheometric (plate-plate) setup in the presence of slip, $P \propto t_0^{-0.03}$, Fig. 3(b).

As a conclusion of this part, the main features of the solid-fluid transition observed in a rheometric flow in the presence of wall slip are equally observed in a unsteady pipe flow.

In spite of its ubiquitous nature and tremendous importance from both a fundamental and applied perspective, the phenomenon of wall slip in pasty materials and dispersions is still under-looked by many researchers, [7]. As Carbopol® gels are concerned, a detail characterisation of their slip properties in slow unsteady pipe flows was, to our best knowledge, insufficiently documented, particularly in regard to the degree of the flow unsteadiness. The time and space resolved measurements of the flow fields based on the **DPIV** technique allowed us to attempt to fill this gap and provide a detailed experimental characterisation of the wall slip phenomenon. Systematic measurements of the slip velocity during controlled pressure ramps with various degrees of steadiness (i.e. for several values of the characterising forcing time t_0) reveal a clear coupling between the irreversible solid-fluid transition and the slip phenomenon. A linear scaling of the slip velocity with the wall velocity gradients is found, Fig. 11. This scaling law is universal in the sense that it does not depend on the flow steadiness and invariantly holds for both the increasing and the decreasing branches of the controlled pressure ramp.

A clear picture of the coupling between the irreversible solid-fluid transition and the slip phenomenon can be obtained by plotting the slip velocity against the wall shear stress, Fig. 12. It is only within the fully yielded regime ($\Delta p > \Delta p_y$) that a Navier-type nearly linear scaling of the slip velocity can be observed. The measurement of the slip coefficient allowed one to estimate the thickness of the lubrication layer responsible for the slip behaviour. The result of this estimate seems to be consistent with previous experimental findings. It is equally interesting to note that this scaling of the slip velocity is practically independent on the flow steadiness (the characteristic forcing time t_0) and whether the driving pressure is increasing or decreasing.

Beyond the main findings briefly highlighted above, the present study also brings a modest contribution from a technical point of view: our approach of correlating **DPIV** measured flow fields with rheometric flow curve data allows a local measurement of the stresses which, in other words, *"converts"* the pipe flow into a table top open flow rheometer. To our best knowledge, this experimental approach is rather new (particularly in the context of viscoplastic flows) and deserves being pursued.

We believe that our experimental findings could trigger several interesting developments at both experimental and theoretical level. A micro flow investigation of the wall slip of Carbopol® gels during unsteady flows over smooth solid surfaces able to simultaneously monitor the flow fields and the micro-gel structure near the solid surface would bring in our opinion a ultimate and direct clarification on the coupling between yielding and slip as well as on the microscopic scale mechanism of slip. Though we are aware that such experiments represent a daunting task, we note that several steps have already been taken in this direction by combining microfluidics with various micro-rheology approaches (diffusion of nano tracers, [26, 25], fluorescent labelling of the gel, [16]).

The success of such a task is strongly conditioned by a better understanding of the physicochemical properties of the Carbopol® gels which would allow developing versatile protocols of fluorescence labelling of the micro-gel particles which would allow the direct visualisation of the gel system under shear.

From a theoretical perspective, our work clearly demonstrates the need of developing new frameworks to understand the unsteady yielding and slip in Carbopol® gels. A modest progress in this direction has been already reported in Ref. [32] where a simple model that can accurately describe the unsteady yielding in a rheometric setup in the absence of wall slip was proposed and validated agains experimental data.

In spite of its ability to describe a large amount of rheological data in both shear and oscillation, within a wide range of polymer concentrations and at various operating temperatures (see Refs. [32, 22, 38]), this model is minimalistic

and can be considered for now as a *"poor man's model"*: it is a scalar model, it has not been derived from first principles, it lacks a thermodynamical validation and, in its present form, it can not account for wall slip.

Future theoretical work is needed to correct these deficiencies and to ultimately attempt to model realistic laminar viscoplastic flows of industrial relevance such as flows around solid objects moving through a gel [33], coating flows, unsteady start-up pipe flows and thermo convective flows.

Acknowledgments

The work was supported by the grant *"ANR ThIM"* generously provided by the *"Agence Nationale de la Recherche"*, France.

M. M. - G. gratefully acknowledges the financial support provided by the *École Polytechnique de l'Université de Nantes* and the hospitality of the *Laboratoire de Thermocinétique* (LTN, UMR 6607), Nantes, France where a substantial part of the work has been completed.

T.B. acknowledges numerous insightful discussions with Professor Ian A. Frigaard on the yielding of Carbopol® gels.

We are indebted to the first referee for her/his comments and suggestions which have significantly contributed to the clarity of our final manuscript.

A. P., T. B. and C. C. are indebted to Christophe Le Bozec and Jérôme Delmas for their help in setting up the experiments.

We gratefully acknowledge the technical support provided by Mr. E. Roussel and Dr. P. Sierro from Thermo Fisher Scientific, Karlsruhe, Germany for the calibration of the nano-torque module installed on the Mars III rheometer and valuable discussions.

References

[1] Barnes, H. A., Feb. 1999. The yield stress–a review or '$\pi\alpha\nu\tau\alpha\ \rho\varepsilon\iota$'–everything flows? Journal of Non-Newtonian Fluid Mechanics 81 (1-2), 133–178.

[2] Barnes, H. A., Walters, K., 1985. The yield stress myth? Rheol. Acta 24, 323–326.

[3] Bertola, V., Bertrand, F., Tabuteau, H., Bonn, D., Coussot, P., 2003. Wall slip and yielding in pasty materials. Journal of Rheology 47 (5), 1211–1226.
URL http://link.aip.org/link/?JOR/47/1211/1

[4] Bingham, E. C., 1922. Fluidity and plasticity. McGraw Hill, London.

[5] Bittleston, S., Ferguson, J., Frigaard, I., 2002. Mud removal and cement placement during primary cementing of an oil well : Laminar non-Newtonian displacements in an eccentric annular hele-shaw cell. Journal of Engineering Mathematics 43, 229–253.
URL http://dx.doi.org/10.1023/A%3A1020370417367

[6] Bonn, D., Denn, M. M., 2009. Yield stress fluids slowly yield to analysis. Science 324 (5933), 1401–1402.
URL http://www.sciencemag.org/content/324/5933/1401.short

[7] Buscall, R., 2010. Letter to the editor: Wall slip in dispersion rheometry. Journal of Rhelogy 54 (6), 1177–1183.

[8] Corvisier, P., Nouar, C., Devienne, R., Lebouche, M., 2001. Development of a thixotropic fluid flow in a pipe. Experiments in Fluids 31 (5), 579–587.
URL http://dx.doi.org/10.1007/s003480100336

[9] Coussot, P., 2005. Rheometry of pastes, suspensions and granular materials. John Willey & Sons.

[10] Curran, S., Hayes, R., Afacan, A., Williams, M., Tanguy, P., 2002. Properties of carbopol solutions as models for yield-stress fluids. Journal of Food Science 67 (1), 176–180.
URL http://dx.doi.org/10.1111/j.1365-2621.2002.tb11379.x

[11] Damianou, Y., Philippou, M., Kaoullas, G., Georgiou, G. C., 2014. Cessation of viscoplastic poiseuille flow with wall slip. Journal of Non-Newtonian Fluid Mechanics 203 (0), 24 – 37.
URL http://www.sciencedirect.com/science/article/pii/S0377025713001870

[12] Denn, M., Bonn, D., 2011. Issues in the flow of yield-stress liquids. Rheologica Acta 50, 307–315, 10.1007/s00397-010-0504-3.
URL http://dx.doi.org/10.1007/s00397-010-0504-3

[13] Divoux, T., Barentin, C., Manneville, S., 2011. From stress-induced fluidization processes to herschel-bulkley behaviour in simple yield stress fluids. Soft Matter 7, 8409–8418.
URL http://dx.doi.org/10.1039/C1SM05607G

[14] Divoux, T., Grenard, V., Manneville, S., Jan 2013. Rheological hysteresis in soft glassy materials. Phys. Rev. Lett. 110, 018304.
URL http://link.aps.org/doi/10.1103/PhysRevLett.110.018304

[15] Divoux, T., Tamarii, D., Barentin, C., Manneville, S., May 2010. Transient shear banding in a simple yield stress fluid. Phys. Rev. Lett. 104, 208301.
URL http://link.aps.org/doi/10.1103/PhysRevLett.104.208301

[16] Gutowski, I., Lee, D., de Bruyn, J., Frisken, B., 2012. Scaling and mesostructure of carbopol dispersions. Rheologica Acta, 1–1010.1007/s00397-011-0614-6.
URL http://dx.doi.org/10.1007/s00397-011-0614-6
[17] Johnson, K. L., 1985. Contact mechanics. Cambridge University press, Cambridge.
[18] Kalyon, Dilhan, M., 2005. Apparent slip and viscoplasticity of concentrated suspensions. Journal of Rheology 49, 621–640.
[19] Ma, X., Duan, Y., Li, H., 2012. Wall slip and rheological behavior of petroleum-coke sludge slurries flowing in pipelines. Powder Technology 230 (0), 127 – 133.
URL http://www.sciencedirect.com/science/article/pii/S0032591012004895
[20] Meeker, S. P., Bonnecaze, R. T., Cloitre, M., 2004. Slip and flow in pastes of soft particles: Direct observation and rheology. Journal of Rheology 48 (6), 1295–1320.
URL http://link.aip.org/link/?JOR/48/1295/1
[21] Moller, P. C. F., Fall, A., Bonn, D., 2009. Origin of apparent viscosity in yield stress fluids below yielding. EPL (Europhysics Letters) 87 (3), 38004.
URL http://stacks.iop.org/0295-5075/87/i=3/a=38004
[22] Moyers-Gonzalez, M., Burghelea, T. I., Mak, J., 2011. Linear stability analysis for plane-poiseuille flow of an elastoviscoplastic fluid with internal microstructure for large reynolds numbers. Journal of Non-Newtonian Fluid Mechanics 166 (910), 515 – 531.
URL http://www.sciencedirect.com/science/article/pii/S0377025711000486
[23] Nagarani, P., Sebastian, B., 2013. Dispersion of a solute in pulsatile non-newtonian fluid flow through a tube. Acta Mechanica 224 (3), 571–585.
URL http://dx.doi.org/10.1007/s00707-012-0753-6
[24] Nguyen, Q. D., Boger, D. V., 1992. Measuring the flow properties of yield stress fluids. Annual Review of Fluid Mechanics 24 (1), 47–88.
URL http://www.annualreviews.org/doi/abs/10.1146/annurev.fl.24.010192.000403
[25] Oppong, F. K., de Bruyn, J. R., 2007. Diffusion of microscopic tracer particles in a yield-stress fluid. J. Non-Newtonian Fluid Mech. 142, 104–111.
[26] Oppong, F. K., Rubatat, L., Frisken, B. J., Bailey, A. E., de Bruyn, J. R., 2006. Microrheology and structure of a yield-stress polymer gel. Phys. Rev. E 73, 041405.
[27] Ovarlez, G., Cohen-Addad, S., Krishan, K., Goyon, J., Coussot, P., 2013. On the existence of a simple yield stress fluid behavior. Journal of Non-Newtonian Fluid Mechanics 193, 68 – 79.
[28] Park, Y. S., Liu, P. L. F., 2010. Oscillatory pipe flows of a yield-stress fluid. Journal of Fluid Mechanics 658, 211–228.
URL http://dx.doi.org/10.1017/S0022112010001667
[29] Pérez-Gonzàlez, J., Lòpez-Durán, J., Marín-Santibañez, B., Rodriguez-Gonzalez, F., 2012. Rheo-piv of a yield-stress fluid in a capillary with slip at the wall. Rheologica Acta, 1–1010.1007/s00397-012-0651-9.
URL http://dx.doi.org/10.1007/s00397-012-0651-9
[30] Phillips, D. A., Forsdyke, I. N., McCracken, I. R., Ravenscroft, P. D., 2011. Novel approaches to waxy crude restart: Part 2: An investigation of flow events following shut down. Journal of Petroleum Science and Engineering 77 (34), 286 – 304.
URL http://www.sciencedirect.com/science/article/pii/S0920410511000830
[31] Piau, J., 2007. Carbopol gels: Elastoviscoplastic and slippery glasses made of individual swollen sponges: Meso- and macroscopic properties, constitutive equations and scaling laws. Journal of Non-Newtonian Fluid Mechanics 144 (1), 1 – 29.
URL http://www.sciencedirect.com/science/article/pii/S0377025707000687
[32] Putz, A. M. V., Burghelea, T. I., 2009. The solid-fluid transition in a yield stress shear thinning physical gel. Rheol Acta 48, 673–689.
[33] Putz, A. M. V., Burghelea, T. I., Frigaard, I. A., Martinez, D. M., 2008. Settling of an isolated spherical particle in a yield stress shear thinning fluid. Phys. Fluids (20), 033102.
[34] Raffel, M., Willert, C. E., Wereley, S. T., Kompenhans, J., September 2007. Particle Image Velocimetry: A Practical Guide (Experimental Fluid Mechanics). Springer; 2nd edition.
[35] Rensing, P. J., Liberatore, M. W., Sum, A. K., Koh, C. A., Sloan, E. D., 2011. Viscosity and yield stresses of ice slurries formed in water-in-oil emulsions. Journal of Non-Newtonian Fluid Mechanics 166 (1415), 859 – 866.
URL http://www.sciencedirect.com/science/article/pii/S0377025711001182
[36] Salmon, J.-B., Becu, L., Manneville, S., Colin, A., 2003. Towards local rheology of emulsions under couette flow using dynamic light scattering. The European Physical Journal E 10, 209–221.
URL http://dx.doi.org/10.1140/epje/i2002-10110-5
[37] Scarano, F., Rhiethmuller, M. L., 2001. Advances in iterative multigrid piv image processing. Exp. Fluids 29.
[38] Weber, E., Moyers-Gonzalez, M., Burghelea, T. I., 2012. Thermorheological properties of a Carbopol gel under shear. Journal of Non-Newtonian Fluid Mechanics 183-184 (0), 14 – 24.
URL http://www.sciencedirect.com/science/article/pii/S0377025712001322
[39] Yoshimura, A., Prud'homme, R. K., 1988. Wall slip corrections for couette and parallel disk viscometers. Journal of Rheology 32 (1), 53–67.
URL http://link.aip.org/link/?JOR/32/53/1